Anal. Chem. **2002,** *74,* 5621−5628

Size Separation of Supermicrometer Particles in Asymmetrical Flow Field-Flow Fractionation. Flow Conditions for Rapid Elution

Karl-Gustav Wahlund* and Andrea Zattoni†

Department of Technical Analytical Chemistry, University of Lund, P.O. Box 124, SE-221 00 Lund, Sweden

The performance of lift-hyperlayer asymmetrical flow field-flow fractionation using rapid elution conditions was tested through the separation of standard polystyrene latex particles of diameters from 2 to 20 μm. Optimization of flowrates was studied not only in order to obtain efficient and rapid separation, but also to work under conditions of various shape and steepness of the axial flow velocity gradient. Using extreme flow conditions, the five widely spaced particle sizes, 20.5-, 15.0-, 9.7-, 5.0-, and 2.0-μm diameter, could be resolved in 6 min, whereas for the narrower size range of 20.5−5.0 μm, 1 min was enough. The size selectivity in the size range 9.7−2.0 μm was studied as a function of flowrates and particle size and was found to be constant. A particle trapping device made it possible to separate particles of sizes >10 μm, which has previously proven to be difficult in asymmetrical channels.

Flow field flow fractionation (flow FFF) is the most versatile method among the various FFF techniques[1,2] and has widely shown its applicability to separate and characterize macromolecular species and particles of different origin over a broad range of sizes. In the conventional, symmetrical flow FFF channel,[3−5] separation is produced by the combined action of an axial flow that carries the analyte along the channel and a perpendicular cross-flow, which passes through the porous walls of the channel and drives the analyte toward the accumulation wall. In asymmetrical flow FFF[6] (AsyFlFFF), only one of the channel walls, the accumulation wall, is porous. Therefore, both the axial flow and the cross-flow are generated from a single inlet flow, which is split in the channel into two perpendicular components. In the past decade, asymmetrical flow FFF has been successfully applied to the separation of a great variety of macromolecular species, such as proteins,[7−16] water-soluble polymers,[7,17−29] colloidal particles,[30] algal and yeast cells,[7,31] ribosomes,[32,33] nucleic acids and plasmids,[7,8] and viruses and their aggregates.[8,34] Generally, in flow FFF, macromolecular, that is, submicrometer, sample components, are separated in the normal mode of elution[2], for which an exact relationship between retention time and particle diffusion coefficient (or hydrodynamic radius) is known. In contrast, for supermicrometer particles, the elution mechanism is referred to as steric-hyperlayer mode,[35] lift-hyperlayer mode[2], or sometimes

* Corresponding author: Fax: +46-46-222-4525. E-mail: Karl-Gustav.Wahlund@teknlk.lth.se.

† Current address: Department of Chemistry "G. Ciamician", University of Bologna, Via Selmi 2, I-40126 Bologna, Italy.

(1) Giddings, J. C. *Science* **1993**, *260*, 1456−1465.
(2) Giddings, J. C. In *Field-Flow Fractionation Handbook*; Schimpf, M., Caldwell, K., Giddings, J. C., Ed.; Wiley-Interscience: New York, 2000, pp 3−30.
(3) Giddings, J. C.; Yang, F. J. F.; Myers, M. N. *Science* **1976**, *193*, 1244−1245.
(4) Wahlund, K. G.; Winegarner, H. S.; Caldwell, K. D.; Giddings, J. C. *Anal. Chem.* **1986**, *58*, 573−578.
(5) Ratanathanawongs-Williams, S. K. In *Field-Flow Fractionation Handbook*; Schimpf, M., Caldwell, K., Giddings, J. C., Ed.; Wiley-Interscience: New York, 2000, pp 257−277.
(6) Wahlund, K. G.; Giddings, J. C. *Anal. Chem.* **1987**, *59*, 1332−1339.
(7) Wahlund, K. G.; Litzén, A. *J. Chromatogr.* **1989**, *461*, 73−87.
(8) Litzén, A.; Wahlund, K. G. *J. Chromatogr.* **1989**, *476*, 413−421.
(9) Litzen, A.; Walter, J. K.; Krischollek, H.; Wahlund, K. G. *Anal. Biochem.* **1993**, *212*, 469−480.
(10) Litzen, A. *Anal. Chem.* **1993**, *65*, 461−470.
(11) Litzen, A.; Garn, M. B.; Widmer, H. M. *J. Biotechnol.* **1994**, *37*, 291−295.
(12) Wahlund, K. G.; Gustavsson, M.; MacRitchie, F.; Nylander, T.; Wannerberger, L. *J. Cereal Sci.* **1996**, *23*, 113−119.
(13) Walse, B.; Kihlberg, J.; Karlsson, K. F.; Nilsson, M.; Wahlund, K. G.; Pinkner, J. S.; Hultgren, S. J.; Drakenberg, T. *FEBS Lett.* **1997**, *412*, 115−120.
(14) Madorin, M.; van Hoogevest, P.; Hilfiker, R.; Langwost, B.; Kresbach, G. M.; Ehrat, M.; Leuenberger, H. *Pharm. Res.* **1997**, *14*, 1706−1712.
(15) Moon, M. H.; Kwon, H.; Park, I. *J. Liq. Chromatogr. Relat. Technol.* **1997**, *20*, 2803−2814.
(16) Wahlund, K.-G. In *Field-Flow Fractionation Handbook*; Schimpf, M., Caldwell, K., Giddings, J. C., Ed.; Wiley-Interscience: New York, 2000, pp 279−294.
(17) Wittgren, B.; Wahlund, K. G.; Derand, H.; Wesslen, B. *Macromolecules* **1996**, *29*, 268−276.
(18) Wittgren, B.; Wahlund, K. G.; Derand, H.; Wesslen, B. *Langmuir* **1996**, *12*, 5999−6005.
(19) Wittgren, B.; Wahlund, K. G. *J. Chromatogr., A* **1997**, *760*, 205−218.
(20) Wittgren, B.; Wahlund, K. G. *J. Chromatogr., A* **1997**, *791*, 135−149.
(21) Schimpf, M. E.; Wahlund, K. G. *J. Microcolumn Sep.* **1997**, *9*, 535−543.
(22) Wittgren, B.; Borgstrom, J.; Piculell, L.; Wahlund, K. G. *Biopolymers* **1998**, *45*, 85−96.
(23) Wittgren, B.; Wahlund, K. G. *Carbohydr. Polym.* **2000**, *43*, 63−73.
(24) Wittgren, B.; Wahlund, K.-G.; Andersson, M.; Arfvidsson, C. *Int. J. Polym. Anal. Charact.* **2002**, *7*, 19−40.
(25) Jenne, F.; Merkle, S.; Naeff, R. *Pharm. Ind.* **2000**, *62*, 64−68.
(26) Viebke, C.; Williams, P. A. *Food Hydrocolloids* **2000**, *14*, 265−270.
(27) Viebke, C.; Williams, P. A. *Anal. Chem.* **2000**, *72*, 3896−3901.
(28) Andersson, M.; Wittgren, B.; Wahlund, K.-G. *Anal. Chem.* **2001**, *73*, 4852−4861.
(29) van Bruijnsvoort, M.; Wahlund, K. G.; Nilsson, G.; Kok, W. T. *J. Chromatogr. A* **2001**, *925*, 171−182.
(30) Othegraven, J.; Piazza, R.; Bartsch, E. *Macromol. Symp.* **2000**, *151*, 515−520.
(31) Pons, M. N.; Litzen, A.; Kresbach, G. M.; Ehrat, M.; Vivier, H. *Sep. Sci. Technol.* **1997**, *32*, 1477−1492.
(32) Nilsson, M.; Birnbaum, S.; Wahlund, K. G. *J. Biochem. Biophys. Methods* **1996**, *33*, 9−23.
(33) Nilsson, M.; Bulow, L.; Wahlund, K. G. *Biotechnol. Bioeng.* **1997**, *54*, 461−467.
(34) Litzén, A.; Wahlund, K. G. *Anal. Chem.* **1991**, *63*, 1001−1007.

10.1021/ac020315s CCC: $22.00
Published on Web 09/21/2002

focusing mode,[36,37] for which the retention time is determined by the equilibrium between the viscous driving force and hydrodynamic lift forces. The latter drives the particles to a narrow band at a certain distance from the accumulation wall.

Rapid separations in flow FFF were realized when peristaltic pumps were abandoned for modern HPLC pumps so that channel inlet flowrates and cross-flow rates of up to and even above 10 mL min^{-1} could be used.[4] This was driven to an extreme when flowrates up to 40 mL min^{-1} were applied in the first flow/steric FFF report.[38]

Several studies have demonstrated the high separation speed and size resolution that can be obtained for supermicrometer particles in the symmetrical flow FFF channels using lift forces,[38−40] but only a few examples of lift-hyperlayer in asymmetrical flow FFF have been reported.[31,41,42] Moreover, there has been no evaluation of how to choose the separation condition, notably the flowrates, in order optimize the particle separation in terms of resolution and time. The optimization for the separation of supermicrometer particles is of primary interest in view of the application of asymmetrical flow FFF to real samples. Because the two important flowrates, the cross-flow and the axial flow, cannot be chosen independently of each other, as opposed to in the symmetrical channel, the adjustments of the flowrates are less simple to comprehend in the asymmetrical version. Another major difference between the two channel versions is that in the asymmetrical channel, there will always be velocity gradients in both the axial flow and the cross-flow.[6] Should it be that the supermicrometer particles are migrating under influence of hydrodynamic lift-forces, the latter should therefore in many cases decrease on approaching the outlet end of the channel; i.e., the retention ratio may not be constant throughout the migration. It cannot even be excluded that the lift forces diminish to 0 if the axial velocity becomes very small close to the outlet. In such cases, supermicrometer particles may enter into migrating in the steric mode,[2,35] that is, in close vicinity to the accumulation wall. A further complication might be expected if particles travel at high elevation from the accumulation wall, where the cross-flow velocity is smaller than it is close to the wall.[6] This could occur for relatively large particles, strongly elevated by lift forces. This might potentially result in size selectivity different from that in a symmetrical channel. Because of the complex interplay of the many factors and because hydrodynamic lift forces have been difficult to predict, it seems that a theoretical analysis of the situation would be very difficult, but that an empirical study on the choice of flow conditions would be important.

In this work, the performance of lift-hyperlayer asymmetrical flow FFF was tested through the separation of standard polystyrene latex particles of diameters from 2.0 to 20 μm. Optimization of the experimental conditions was studied in terms of flowrates not only to obtain efficient and rapid separation, but also to work under conditions of varying steepness of the axial flow velocity gradient. The size selectivity was studied as a function of flowrates and particle size. Additionally, technical improvements made it possible to separate particles of sizes >10 μm, which has previously proven to be difficult in asymmetrical channels.

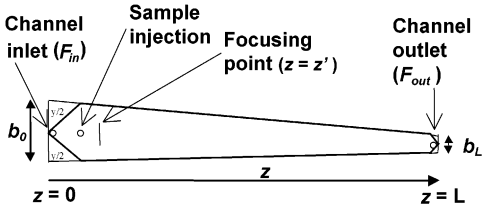

Figure 1. Illustration of the trapezoidal asymmetrical flow FFF channel.

EXPERIMENTAL SECTION

Asymmetrical Flow FFF System. The trapezoidal asymmetrical channel was assembled and managed as described earlier.[9,17,34] The channel, illustrated in Figure 1, was cut out from a poly(tetrafluoroethylene) spacer and had a trapezoidal geometry, with a length, L, of 28.5 cm and a breadth at the inlet and outlet (b_0 and b_L) of 2.0 and 0.5 cm, respectively, giving $b_0/b_L = 4.0$. The area y cut off at the inlet was 2.0 cm^2, and the total area of the membrane enclosed by the spacer was 33.6 cm^2. The channel thickness was calibrated with ferritin[10] as 0.0110 cm, which gave a channel volume of 0.383 cm^3. The focusing point was set at 1.0 cm downstream of the injection inlet (i.e., at $z' = 3.0$ cm) by injecting a colored sample (bromophenol blue). The channel was held with its axis in a vertical position.

A regenerated cellulose ultrafiltration membrane, type Nadir UF-C10 (Hoechst AG, Wiesbaden, Germany) made the accumulation wall. It had a 10 000 molecular weight cutoff. The carrier flow was generated by a 422 HPLC pump (Kontron Instruments, Milan, Italy), and the sample injection pump was a CMA100 model syringe pump (MCA/Microdialysis, Stockholm, Sweden). Two motor-driven switching valves, denoted V1 and V2 in Figure 2, directed the carrier flow and the operating modes. V1 was a Valco WE-C8WPK 2-position, 8-port valve, and valve 2 was a Valco CST4UW 4-position 10-port valve (Vici, Valco Europe, Schenkon, Switzerland). Both axial flowrate and cross-flow rate were measured by two model FL4POC liquid flow meters (Phase separations, Queensferry, U.K.) with a measuring range of up to 10 mL × min^{-1}. Two needle valves were used to regulate the focusing point and the channel outlet flowrate. For the focusing point, it was a Whitey SS-22RS2 "22" series Micrometering valve (Whitey Co., Highland Heights, OH) (N1), and for the channel outlet flowrate, it was a Hoke 1656G2YA Micromite Forged Metering Valve (Hoke, Cresskill, NJ) (N2). The spectrophotometric detector was a Jasco UV-970 (Jasco corporation, Tokyo, Japan) operating at 420 nm. The detector signal was captured by GynkoSoft Chromatography Data System version 5.30 computer software (Softron, Germering, D), which also was used for computer control of the pump setting and the switching valves. Sample injection was performed through a Rheodyne Sample Injector model 9125 (Rheodyne, Cotati, CA), with a 20-μL sample loop. A 47-mm diameter stainless steel filter holder (Millipore, Bedford, MA)

(35) Caldwell, K. D. In *Field-Flow Fractionation Handbook*; Schimpf, M., Caldwell, K., Giddings, J. C., Ed.; Wiley-Interscience: New York, 2000, pp 79−94.
(36) Janca, J.; Chmelik, J. *Anal. Chem.* **1984**, *56*, 2481−2484.
(37) Chmelik, J. *J. Chromatogr. A* **1999**, *845*, 285−291.
(38) Giddings, J. C.; Chen, X. R.; Wahlund, K. G.; Myers, M. N. *Anal. Chem.* **1987**, *59*, 1957−1962.
(39) Chen, X. R.; Wahlund, K. G.; Giddings, J. C. *Anal. Chem.* **1988**, *60*, 362−365.
(40) Ratanathanawongs, S. K.; Giddings, J. C. *Chromatographia* **1994**, *38*, 545−554.
(41) Moon, M. H.; Kim, K.; Byun, Y.; Pyo, D. *J. Liq. Chromatogr. Relat. Technol.* **1999**, *22*, 2729−2740.
(42) Moon, M. H.; Williams, P. S.; Kwon, H. *Anal. Chem.* **1999**, *71*, 2657−2666.

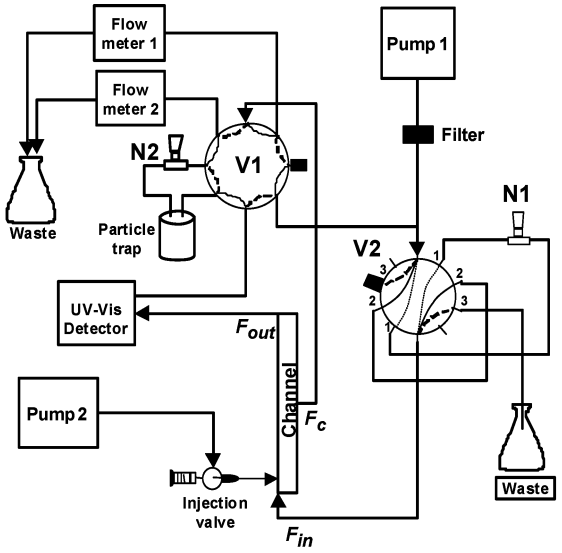

Figure 2. Schematic illustration of the instrumental setup. The channel was held in a vertical position to avoid sedimentation forces from contributing to retention. Pump 1 generates the carrier flow and pump 2, the injection flow. The switching valves V1 and V2 control the carrier path through the system in the elution and relaxation/focusing modes, respectively. The arrows indicate the flow directions in the elution mode. The position of the focusing point is controlled by the needle valve N1, which regulates the magnitude of channel flowrates in the focusing mode. The needle valve N2 regulates the channel outlet flowrate in the elution mode. A particle trap was placed before N2 to prevent its clogging. Flow meters 1 and 2 monitor the cross-flow rate and the channel outlet flowrate, respectively.

equipped with a 0.45-μm regenerated cellulose filter, model SM 11606 (Sartorius AG, Göttingen, Germany), was connected on-line directly after the carrier pump. A particle trap was positioned after the detector outlet between the valves V1 and N2 in order to prevent large particles from entering the needle valve N2. The particle trap was modified from a bubble trap from FFFractionation LLC (Salt Lake City, UT). The filter was the same as that used right after the pump and was cut to fit the size of the trap. The injection flowrate was set to 100 μL/min, and injection volume was 60 μL. The injection and relaxation/focusing procedure lasted for a total of 1 min with the pump set at 2 mL min^{-1}. For the elution phase, the inlet channel flowrate F_{in} was set at different values from 2 to 10 mL $\times$ min^{-1}. At the end of the elution, a 1-min rinsing procedure in a backflushing mode was performed at 6 mL $\times$ min^{-1}.

Samples and Chemicals. Sample particles were seven polystyrene latex standards in the size range 2−20 μm (Duke Scientific Co., Palo Alto, CA, or Polysciences, Inc., Warrington, PA). The specifications are given in Table 1. The carrier liquid was Milli-Q water (Millipore, Bedford, MA) with 0.05% sodium dodecylsulfate (SDS) (Sigma chemical, St. Louis, MO) added to improve sample dispersion and 0.01% sodium azide (Merck, Darmstadt, Germany) as a bactericide. Particles were dispersed in the carrier at concentrations varying from 0.01 to 0.13% w/v. Ferritin for channel thickness calibration was type I from horse spleen (Sigma, St. Louis, MO).

RESULTS AND DISCUSSION

Particle Trap. Large particles can be difficult to make pass through the outlet needle valve N2 (Figure 2), causing the valve to be constricted and finally clogged. Eventually, a drop to nearly 0 flowrate of the channel outflow during elution can occur. The same problem was reported previously,[43] which prevented the separation of particles larger than 10 μm. To avoid valve clogging in the present study, a particle trap unit was placed after the detector and before the needle valve N2. The particle trap contained a filter having a pore size that makes it retain micrometer-sized particles.

Table 1. Polystyrene Particles Studied

source	nom diam (μm)	cert diam (μm)	SD (μm)	batch concn (% w/w)
Duke	2.0	2.013	0.025	0.45
Polybead	3.1	3.135	0.146	2.6
Polybead	4.6	4.562	0.209	2.6
Duke	5.0	5.010	0.038	0.31
Duke	9.7	9.685	0.064	0.20
Duke	15.0	15.00	0.07	0.28
Duke	20.5	20.49	0.20	0.33

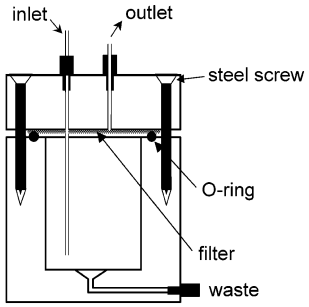

Figure 3. Particle trap. Height, 7 cm; inner diameter, 4 cm; inner volume, 45 mL. The inlet tube enters the trap through a hole of the same diameter cut in the filter. The cellulose filter seals around the cut hole by adhesion to the top part through the pressure in the trap, thereby preventing the particles from entering the outlet tube.

A scheme of the particle trap is shown in Figure 3. The trap was completely filled with carrier (~45 mL), and its function was to allow the sample particles to settle to the bottom and thereby prevent filter occlusion. The trap has the advantages of a large volume and large filter surface area. This reduces the risk of clogging the filter. The trap can be quickly emptied and cleaned through the bottom hole. This was done after ~50 runs.

Choice of Flowrate Regimes: Calculation of Velocity Gradients. In separating supermicrometer particles by flow FFF, the operating mode has always been observed to be the steric or lift-hyperlayer modes[31,38−41,43−45] characterized by elution of larger particles before smaller. In asymmetrical flow FFF (AsyFlFFF), however, it is not obvious how to rationalize the choice of flow rates in view of the complex interrelationship between the three channel flow rates (a single inlet, and two outlets) and, in addition, the lack of theory for hydrodynamic lift-forces. Because the cross-flow rate directly determines the cross-flow force and indirectly the axial transport velocity and, therefore, any hydrodynamic lift force, the choice of flowrates will have to be influenced by the geometry of the channel. In this study, we used the length-breadth geometry that has been commonly applied for trapezoidal channels[34] in AsyFlFFF, as illustrated in Figure 1. For a different geometry, including the thickness, values of the flowrates other

(43) Moon, M. H.; Kwon, H.; Park, I. *Anal. Chem.* **1997**, *69*, 1436−1440.

than those chosen in this study need to be used to obtain similar results.

In AsyFlFFF, it is convenient to express the chosen experimental conditions in terms of the flowrate F_{in} and the ratio F_c/F_{out}.[6] In the normal mode of flow FFF operation, these have an accurately predicted influence on the retention times according to the retention theory so that the retention times for well-retained components are independent of F_{in} but are strongly dependent on F_c/F_{out}.[6,16] However, because it was expected in the present study that the supermicrometer particles were to be eluted under influence of hydrodynamic lift forces, they would migrate in the lift-hyperlayer mode.[2,38−40,46,47] The lift force is driven by the axial velocity, and because the latter is known to form a gradient of various shapes[34] in asymmetrical channels, as opposed to in symmetrical channels, it may be anticipated that, for example, where the gradient has its lowest value, there is a risk that the lift force may not be significant and, thus, that the particles may start to migrate close to the accumulation wall in the steric mode. This could lead to a different retention behavior of the particles, because while they are migrating in the steric mode, they are in close vicinity to, or even contacting, the accumulation wall, which increases the chances for particle−wall interactions.

Another difference from symmetrical channels is that there is also a gradient in the cross-flow velocity so that the latter reaches a nearly constant maximum value only in the close vicinity of the accumulation wall, that is, below 0.1 of the channel thickness.[6] It can be concluded that for particles migrating above this level, that is, very weakly retained particles, the gradient in cross-flow velocity could start to influence the results. If particles are lifted to such high elevations, they may thus enter into the slower part of this gradient, and the balance between the cross-flow force and the lift force may then be different from otherwise, possibly leading to different size selectivity.

The character of the axial velocity gradient can be calculated,[34] and the trapezoidal asymmetrical channel shape was actually introduced to make the gradient less pronounced than it is in a rectangular asymmetrical channel.[34] It was concluded that the gradient shape is dependent on both the geometry of the channel and the magnitudes of the cross-flow rate, F_c, and the inlet flowrate, F_{in}, so that for a fixed geometry, the velocity gradient changes its character if the flowrates are changed. A further conclusion was that the velocity gradient can never become 0; i.e., constant axial flow velocity cannot be obtained in a trapezoidal channel, because this would require some nonlinear decrease of the breadth.[34] Later, it was shown that an exponential decrease would give such constant flow velocity, however, only for a given set of the flowrates.[48] This is when the ratio of channel inlet flowrate to outlet flowrate, F_{in}/F_{out}, equals the ratio of b_0/b_L, that is, the ratio of inlet to outlet breadth. Moreover, it was shown that if such flow rate conditions were to be applied in a trapezoidal channel, it would give the least variation in axial flow velocity along length z and would be characterized by equal flow velocities at the channel inlet and outlet, with a minimum at 0.69 of the total channel length.

The axial flow velocity gradient may not be an experimental problem, except if the axial velocity becomes so low that the band broadening of sample components is dominated by axial diffusion rather than by nonequilibrium effects.[10,34] This would not be a problem with micrometer particles because of their low diffusion coefficients. It is also possible that sample components become effectively immobilized at the accumulation wall if the axial velocity falls below a certain "threshold" value in comparison to the cross-flow velocity. Such threshold effects have been observed for submicrometer macromolecular components[4] but are not usually seen today when high-speed separations are performed using relatively high channel velocities in relation to the cross-flow velocity.[4] Yet, related immobilization phenomena have been seen for supermicrometer particles in steric/hyperlayer flow FFF in symmetrical channels.[38] Still, therefore, the velocity gradient in the asymmetrical channel axial flow might create this effect.

The axial velocity gradients may be of particular interest to consider in performing lift-hyperlayer AsyFlFFF of supermicrometer particles (cf. ref 49). The lift forces should directly depend on the magnitude of the axial velocity, and if anywhere along the channel the velocity drops below some particular value so that the lift forces are unable to counter the drag of the cross-flow, the particles may assume the steric mode, which often tends to high retention levels for small particles. They may then come in contact with the accumulation wall and become practically immobilized in the channel, maybe as a result of interactions with the accumulation wall.[49] This might be the reason for nonelution of 2.0-μm particles in 510-μm-thick channels.[38]

Figure 4 shows the cross-sectional mean axial velocity gradient of the carrier liquid along the channel under a broad range of different flowrate conditions. The graphs were calculated by[48]

$$\langle v\rangle_z = \langle v\rangle_0\left\{1 - \frac{2(1 - F_{in}/F_{out})}{1 + b_L/b_0} \times \left[\frac{z}{L} - \frac{(1 - b_L/b_0)}{2}\frac{z^2}{L^2}\right]\right\} \times \left[1 - \left(\frac{b_L}{b_0}\right)\frac{z}{L}\right]^{-1} \quad (1)$$

where z is the coordinate along the channel, $\langle v\rangle_z$ is the cross-sectional mean velocity at distance z, and $\langle v\rangle_0$ is the cross-sectional mean flow velocity at the channel inlet. F_{in} and F_{out} indicate the channel flowrates at the channel inlet and outlet, respectively.

The condition, $F_{in}/F_{out} = b_0/b_L$,[48] that gives the least variation of axial flow velocity is fulfilled in Figure 4A where the $F_{in}/F_{out} = b_0/b_L = 4.00$ and $F_c/F_{out} = 3.00$. Then it can be calculated that the velocity has the same value at the channel inlet as at the outlet and a minimum at 2/3 L (0.69 according to Williams[48]), with a 20% velocity drop in between. It can be shown that these results are independent of the F_{in} value. For $F_c/F_{out} < 3$, the velocity at the channel outlet is higher than at the inlet (Figure 4"0 ", cf. ref 34). For $F_c/F_{out} > 3$, the velocity gradient tends to become much steeper with less curvature (Figure 4B−E) so that the drop in velocity from inlet end to outlet end becomes as large as 81% at $F_c/F_{out} = 20$ and 86% at $F_c/F_{out} = 30$. The lowest axial velocity, 20

(44) Ratanathanawongs, S. K.; Giddings, J. C. *Anal. Chem.* **1992**, *64*, 6−15.
(45) Liu, M. K.; Williams, P. S.; Myers, M. N.; Giddings, J. C. *Anal. Chem.* **1991**, *63*, 2115−2122.
(46) Giddings, J. C. In *Sep. Sci. Technol.* 1983; Vol. 18, pp 765−73.
(47) Barman, B. N.; Ashwood, E. R.; Giddings, J. C. *Anal. Biochem.* **1993**, *212*, 35−42.
(48) Williams, P. S. *J. Microcolumn Sep.* **1997**, *9*, 459−467.
(49) Williams, P. S.; Xu, Y. H.; Reschiglian, P.; Giddings, J. C. *Anal. Chem.* **1997**, *69*, 349−360.

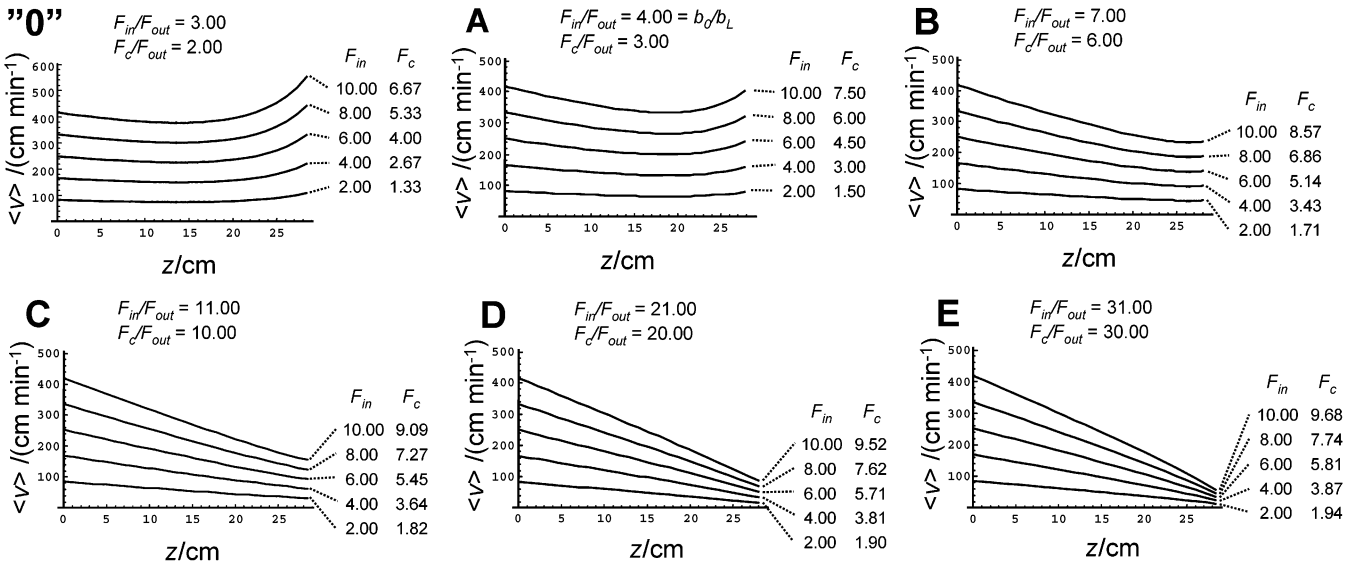

Figure 4. Cross-sectional mean axial flow velocity calculated by eq 1 as a function of the distance, z, from the channel inlet at six different combinations of the flowrates F_{in}, F_c, and F_{out} (mL × min^{-1}) as labeled in parts "0" and A−E. In all cases, $b_0/b_L = 4.00$. The conditions in A demonstrate the least possible change of the axial velocity along the channel.

cm min^{-1}, applied in the results reported in this work is obtained for $F_{in} = 4.00$ in Figure 4D and $F_{in} = 8.00$ in Figure 4E.

Choice of Flowrate Regimes: Experiments. Figure 5 shows a series of fractograms obtained from the separation of a mixture of 2.0-, 3.1-, 4.6-, 5.0-, and 9.7-μm particles. The void time, t^0, was calculated through the expression[34]

$$t^0 = \frac{V^0}{F_c}\ln\left\{1 + \frac{F_c}{F_{out}}\left[1 - \frac{w\left(b_0 z' - \frac{b_0 - b_L}{2L}z'^2 - y\right)}{V^0}\right]\right\} \quad (2)$$

In all cases, a good correspondence between the calculated void time and the experimental "void peak" retention time was found. The channel inlet flowrate ranged from 2 to 10 mL × min^{-1} and F_c/F_{out}, from 3 to 20. These conditions correspond to those applied in the calculations of Figure 4A−D. Since the retention time for a given size was observed to increase with increasing F_c/F_{out} and decreasing F_{in}, the flow conditions were varied in a wide range until the peak from the largest particle could not be resolved from the void peak (Figure 5A, $F_c/F_{out} = 3$, $F_{in} = 6$) and until the smallest particle peak was not observable (Figure 5D, $F_c/F_{out} = 20$). In Figure 5C ($F_c/F_{out} = 10$), the highly retained 2.0-μm particles show poor recovery relative to the other particle sizes. At the even higher retention level (t_r/t^0), in Figure 5D, they disappeared. The latter may be caused by the very high cross-flow rate so that the particles are eluted at a very close distance from the accumulation wall. Therefore, they might have approached the steric mode in which side effects may cause problems (adhesion to the wall, the retardation effect[50]).

It is clear that the conditions in Figure 5C are the best in terms of resolution per time unit and peak shape for the complete set of particle sizes in the range 2.0−10 μm. In Figure 5A, the largest particle is not well-resolved from the void time, whereas the smallest particles are, and within short retention time, as well. On the other hand, in Figure 5D the largest particle was well-resolved under a relatively high retention level, whereas one had to sacrifice the smallest particle, because this was noneluted. This means that it is difficult to obtain conditions enabling good retention, high resolution, and high recovery of both large and small particles from a wide range of particle sizes, such as 2−20 μm.

In principle, this effect can be counteracted by applying, in addition, a sedimentation field, which will reduce the size selectivity. This can be obtained by tilting the channel or by keeping it in horizontal position.[39] The result would be that larger particles become more retained relative to smaller particles (the size-selectivity decreases) so that the resolution from the void peak in the early part of the fractogram improves. Care must be observed if this is attempted on particles of rather high density, because the substantial increase in the transversal force (flow field + sedimentation field) might be difficult to counteract in practice by the necessary increase in the axial flow velocity needed to keep a reasonable retention level and avoid nonelution.[39]

There is no evidence of any general detrimental influence on the separation performance by the drastic velocity changes demonstrated in Figure 4. It has been suggested that adhesion and adsorption to the membrane can contribute to nonelution conditions.[38] The conditions in Figure 4E at $F_{in} = 2$ mL × min^{-1}, where the lowest axial velocity is obtained and the highest cross-flow is operating, would be most prone to this effect. This may explain the result in Figure 5D in which the 2.0-μm particle is invisible, and the 3-μm particle has a skewed peak shape.

Figure 6 shows fractograms when the particle size range was extended to include 15- and 20-μm particles but with exclusion of the 2-μm particle. A mixture of 5.0-, 9.7-, 15.0-, and 20.5-μm particles was eluted at $F_{in} = 8$ mL × min^{-1} with F_c/F_{out} ranging from 8 to 30. In Figure 6A, the flowrates have been optimized for a rapid separation of 5- to 20-μm particles with a total retention time below 1 min. At $F_c/F_{out} = 30$ (Figure 6C), the 20-μm particle is even

(50) Williams, P. S.; Koch, T.; Giddings, J. C. *Chem. Eng. Commun.* **1992**, *111*, 121−147.

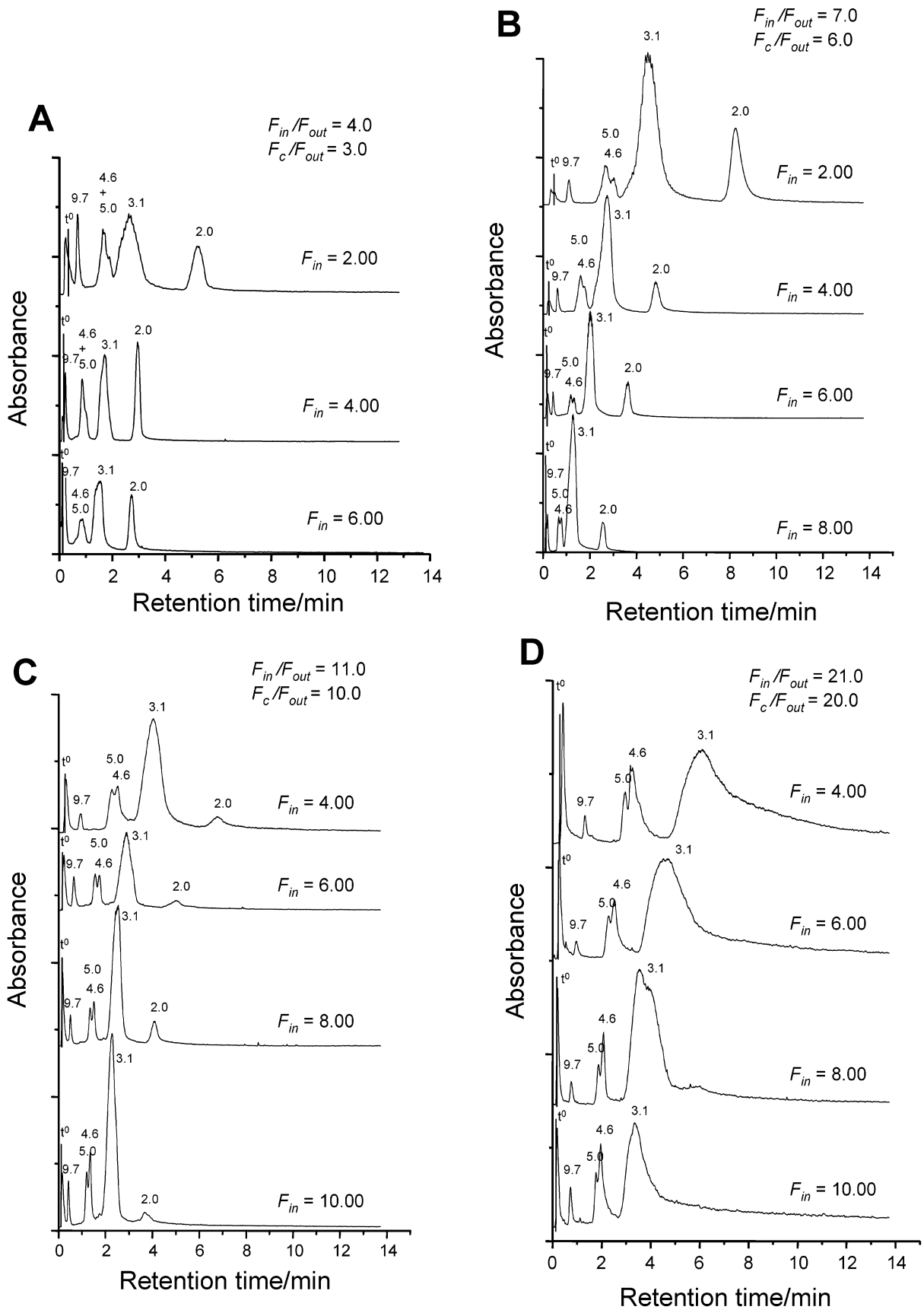

Figure 5. Fractograms of polystyrene particles in the diameter range 2−10 μm. The flow conditions were chosen to coincide with those in Figure 4A−D. Unit for the flowrates F_{in}, F_c, and F_{out}: mL × min^{-1}. The numbers above the peaks indicate the particle diameter.

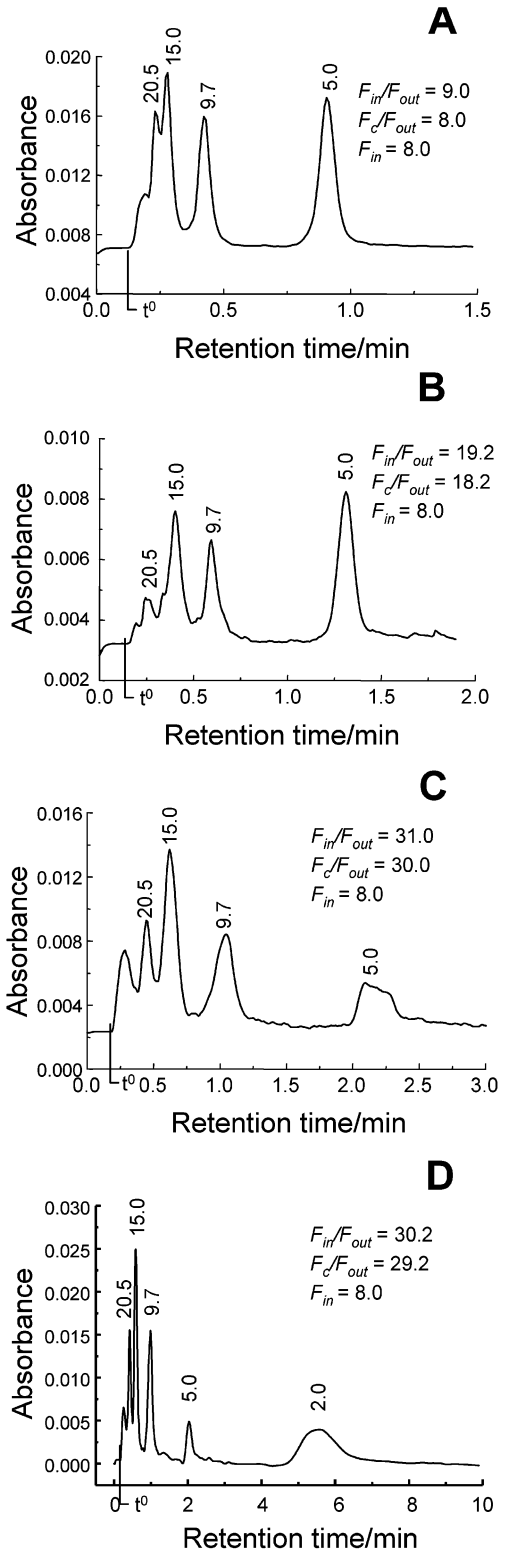

Figure 6. Fractograms of polystyrene particles in the diameter range 5−20 μm and 2−20 μm. The flowrates used in C and D correspond to the conditions in Figure 4E.

better resolved, but the 5-μm peak has an irregular shape, probably due to interaction with the membrane. Finally, in Figure 6D is shown a fractogram performed at 8 mL × min^{-1} and F_c/F_{out} = 29, with the full size range of 2.0−20.5-μm particles. However, note that the good peak shape of the 2.0-μm particles is normally not very reproducible in these conditions.

Figure 6D represents the rather extreme flow conditions (F_c/F_{out} = 29) that are necessary to obtain good resolution among both the largest and the smallest particles. The main reason is that the large particles are subject to substantial lift, which demands compensation by high cross-flow rates to push the particles to retention times beyond the void time. It is a limitation of the asymmetrical channel that it is rather difficult to obtain good retention of particles larger than 15 μm, even if a high cross-flow is applied. The main reason is that the high cross-flow necessitates that the axial channel inlet flowrate is high. This contributes to high lift effects in the early part of the channel. Perhaps a remedy for this could be to operate with thicker channels.

Size Selectivity. The size selectivity has a large influence on the resolution between different particle sizes. Moreover, in certain applications, a numerical value for the size selectivity is needed as a quantitative measure of the relationship between particle size and retention time. One example is the calculation of particle diameter polydispersity.[51] Another is the application of the method of particle size and sample amount distribution, PSAD, in FFF.[52−55] The usual definition of the diameter-based selectivity, S_d, is[56]

$$S_d = \left|\frac{\partial \log t_r}{\partial \log d}\right| \tag{3}$$

where d is the particle diameter. For steric and lift-hyperlayer mode, in which the retention time decreases with increasing diameter, it follows that

$$\log t_r = -S_d \log d + \log t_{r1} \tag{4}$$

Here t_{r1} is the retention time of a particle of unit diameter. Figure 7 shows a characteristic result of a "selectivity plot" in the size range 2.0−9.7 μm according to eq 4 using data selected from those collected in Table 2. These were taken from the fractograms reported in Figure 5 with retention times measured at the peak maxima. A deconvolution of the incomplete fractionation between the 4.5- and 5.0-μm particles indicated that the measured peak maximum retention times showed no significant error. The plots show good linearity. In some cases, at low F_c/F_{out} and high F_{in}, the 9.7-μm particle was not included in the regression, because it was not well-resolved from the void peak. The size selectivity is on average 1.28 ± 0.05 SD. The slight differences in observed selectivity between the various flow conditions seem not to be significant. Similar values of the size selectivity and the same good linearity in the selectivity plot, were obtained in the size range 5.0−20.5 μm (5.0-, 9.7-, 15.0-, and 20.5-μm particles). For example, S_d was 1.35 with conditions (F_{in}/F_{out} = 15.7; F_c/F_{out} = 14.7; F_{in} =

(51) Ratanathanawongs, S. K.; Giddings, J. C. *J. Chromatogr.* **1989**, *467*, 341−356.
(52) Reschiglian, P.; Melucci, D.; Torsi, G. *Chromatographia* **1997**, *44*, 172−178.
(53) Reschiglian, P.; Melucci, D.; Zattoni, A.; Torsi, G. *J. Microcolumn Sep.* **1997**, *9*, 545−556.
(54) Reschiglian, P.; Melucci, D.; Torsi, G.; Zattoni, A. *Chromatographia* **2000**, *51*, 87−94.
(55) Reschiglian, P.; Melucci, D.; Zattoni, A.; Mallo, L.; Hansen, M.; Kummerow, A.; Miller, M. *Anal. Chem.* **2000**, *72*, 5945−5954.
(56) Myers, M. N.; Giddings, J. C. *Anal. Chem.* **1982**, *54*, 2284−2289.

Table 2. Experimental Data and Size-Selectivity from Triple Runs of the Fractograms of Figure 5[a]

F_{in} (mL × min^{-1})	F_c (mL × min^{-1})	F_{out} (mL × min^{-1})	F_c/F_{out}	S_d	SD	log t_{r1}	SD	$r^{2\,b}$	n[c]
2	1.52	0.5	3	1.26	0.03	1.12	0.02	0.994	15
4	3.05	1.01	3	1.35	0.04	0.92	0.02	0.997	12
6	4.58	1.52	3	1.31	0.05	0.83	0.03	0.991	12
2	1.74	0.29	6	1.26	0.02	1.29	0.02	0.998	15
4	3.49	0.58	6	1.29	0.04	1.09	0.02	0.997	15
6	5.24	0.87	6	1.33	0.05	0.97	0.02	0.994	15
8	6.98	1.16	6	1.46	0.05	0.85	0.02	0.998	12
4	3.7	0.37	10	1.26	0.02	1.23	0.01	0.999	15
6	5.55	0.55	10	1.30	0.01	1.10	0.01	0.999	15
8	7.41	0.74	10	1.32	0.05	1.04	0.02	0.996	15
10	9.26	0.92	10	1.25	0.03	0.96	0.02	0.995	12
4	3.88	0.19	20	1.19	0.07	1.37	0.07	0.976	12
6	5.82	0.29	20	1.35	0.03	1.31	0.04	0.995	12
8	7.76	0.38	20	1.33	0.02	1.20	0.03	0.999	12
10	9.7	0.48	20	1.33	0.02	1.18	0.02	0.999	12

[a] Linear regression according to eq 4. [b] r^2 is the correlation coefficient. [c] Number of data.

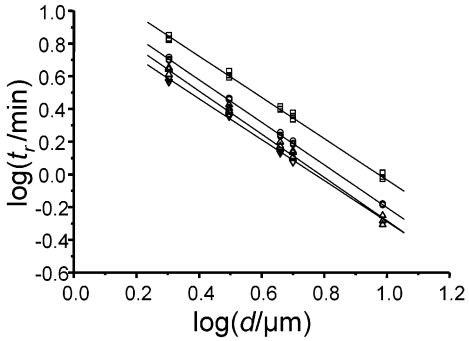

Figure 7. Size selectivity plot for particle sizes 2.0, 3.1, 4.6-, 5.0, and 9.7 μm corresponding to the fractogram in Figure 5C. Data taken from Table 2 for the case $F_c/F_{out} = 10.0$. $F_{in} = 4.00$ (□×ff), 6.00 (○), 8.00 (△), and 10.00 (▼) mL × min^{-1}.

8.0) close to those in Figure 6B so that the 15.0- and 20.5-μm particles were well enough resolved.

The size selectivity is comparable to or slightly higher than analogous values reported for polystyrene particles in symmetrical FlFFF.[51,55] In asymmetrical flow FFF, there is one report on separation of supermicrometer polystyrene standard particles in the size range 3−10 μm.[43] The stopless mode of frit−inlet injection had been applied, and it can be shown that the selectivity was only 0.82. Moreover, in comparison to that study, it can be noted that in the present study, the fractionation time, up to and including the 3-μm particle, has been reduced up to 40% without loss of resolution.

ACKNOWLEDGMENT

This work was supported by the Swedish Natural Science Research Council, the Swedish Research Council for Engineering Sciences, and the European Commission project INCO-Copernicus IC15-CT980909. This work was presented at the 22nd International Symposium on Chromatography, Rome (Italy), September 13−18, 1998, and the Eighth International Symposium on Field-Flow Fractionation, Paris (France), September 6−8, 1999.

Received for review May 9, 2002. Accepted August 7, 2002.

AC020315S